JOURNAL OF PROPULSION AND POWER
Vol. 17, No. 1, January–February 2001

Transient Force Reduction in Electromechanical Actuators for Thrust-Vector Control

Dale E. Schinstock*
The University of Tulsa, Tulsa, Oklahoma 74014-3189
Douglas A. Scott†
Purdue University, West Lafayette, Indiana 47907
and
Tim A. Haskew‡
The University of Alabama, Tuscaloosa, Alabama 35487-0276

There is a move within the aerospace community to use electromechanical actuators (EMA) in thrust-vector control (TVC) applications. However, shock-wave forces that occur during startup and shutdown of unthrottled TVC rocket engines excite resonance in the mechanical dynamics. This results in very large forces transmitted through the actuator. Additionally, with traditional compensation, the position control system must be designed with low bandwidth because of the typically low resonant frequency. Dynamic force feedback (DFF) compensation is proposed to reduce the effects of resonance. Utilizing a motor position sensor and a load cell in the actuator mount, a proportional-integral-derivative (PID) position control loop is closed in parallel with a force control loop to provide resonance reduction and transmitted force reduction. This allows higher position control bandwidths while reducing the transmitted forces. The controller design methodology uses two independent loop-shaping procedures, which are separated by their effective frequency ranges. The techniques are validated with experimental data from an EMA-TVC simulator, showing improvements in both the position control and the transmitted forces. Additionally, the controller is shown to be robust with respect to variation in the resonance.

Nomenclature

b_1	=	equivalent translational damping of the actuator
b_2	=	equivalent translational damping of the engine
F	=	force equivalent to the developed motor torque
F_d	=	equivalent disturbance force
F_t	=	force transmitted in the spring and actuator
$G_{\text{olf}}(s)$	=	open-loop transfer function for force
$G_{\text{olp}}(s)$	=	open-loop transfer function for position
I_c	=	commanded motor current
j	=	imaginary unit
k	=	lumped equivalent spring rate
k_b	=	motor back emf constant
k_f, p_f	=	gain and break point of the DFF filter
k_p, k_i, k_d	=	PID position controller gains
k_t	=	motor torque constant
m_1	=	actuator's equivalent translational mass
m_2	=	pendulum's equivalent translational mass
N	=	ratio of motor rotation to nut translation
x	=	rigid body translation
x_c	=	commanded position
x_1	=	equivalent translation of the motor rotation
x_2	=	equivalent translation of the pendulum rotation
z_1, z_2	=	PID controller zeros
ζ	=	damping ratio
ω_{bwf}	=	closed-loop force control bandwidth
ω_{bwp}	=	closed-loop position control bandwidth
ω_{res}	=	resonant frequency of mechanical system

Received 14 December 1998; revision received 10 June 1999; accepted for publication 16 August 1999.

*Assistant Professor, Mechanical Engineering Department, 600 South College Avenue; dale-schinstock@utulsa.edu.
†Research Assistant, Mechanical Engineering Department, 1288 Mechanical Engineering Building.
‡Associate Professor, Electrical and Computer Engineering Department.

Introduction

ADVANCES in the technologies associated with electromechanical actuators (EMA), such as brushless motors, power electronics, and motor control methods, have made these systems a viable alternative to hydraulics in high-power applications. As a result, NASA and several aerospace manufacturers are exploring the use of EMAs in high-power and flight-critical applications on aircraft and spacecraft. One such application is thrust-vector control (TVC) of rocket engines. NASA/Marshall Space Flight Center is currently developing EMAs to replace the hydraulic servo actuators used on space vehicles with TVC. The Power-by-Wire[1] program in the U.S. Air Force and the commitment of NASA to use all-electric actuation on future spacecraft[2] are indications of the transition to EMA. The X-33 Advanced Technology Demonstrator is an example of an electric spacecraft. Increased reliability, reduced weight and volume of the integrated power and actuation system, and decreased maintenance requirements are all cited as potential benefits of using EMA.

Unfortunately, the benefits of EMA do not come without some associated concerns or risks. Perhaps the most difficult problem to overcome will be the design and integration of the power generation and/or storage systems that are required. However, the control systems for EMA are also a significant concern. As in many manufacturing systems,[3] the coupling between the motor and load (engine) proves to be a source of unwanted resonance in EMA-TVC systems. Disturbance forces that occur during startup and shutdown of unthrottled TVC engines excite resonance and, therefore, must be removed through compensation. Additionally, with traditional compensation the position control system of these EMAs must be designed with a bandwidth much less than any significant resonance in the mechanical system.

This paper focuses on the control of EMA in TVC applications where large engine start and stop transients exist. A NASA EMA-TVC simulator is used for experimental validation of the techniques and models developed for control. The principle control addition is the use of a dynamic force feedback (DFF) controller to reduce the effects of transient forces. The basic principle behind the DFF compensator is to incorporate a force feedback loop for transient force

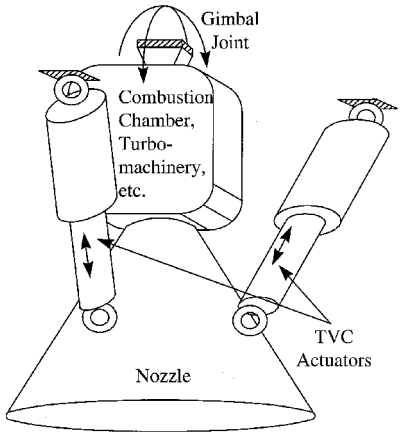

Fig. 1 TVC system.

compensation. At other periods of operation, where the transient forces do not occur, a traditional PID loop dominates the dynamics. The two control regimes are separated by frequency; force control is only dominant when the resonance is excited either by the outside disturbance forces or by position commands. It will be shown experimentally and theoretically that the actuator's transmitted forces are reduced considerably and that the EMA position response is improved with the addition of the DFF compensator.

TVC involves the manipulation of engine thrust in the attitude control of a vehicle. Figure 1 illustrates the placement and function of the actuators for TVC. As the actuators extend and contract, the rocket engine pivots about a gimbal joint. Through coordination of the two actuators, the thrust can be directed as needed to control the movement of the vehicle. Each actuator requires tight, independent position control to accomplish this task. The actuator's working load is mainly inertial, attributed to the mass of the engine. However, as mentioned before, large combustion transients are experienced at engine startup and shutdown,[4] complicating controller design. It is desirable to develop an EMA controller that can provide accurate, high-bandwidth engine position control while at the same time reducing the forces on the actuator during startup and shutdown. These two objectives are difficult to achieve because they are opposing in nature; both position and force cannot be controlled independently using only a single input (i.e., motor torque).

Little published research is available on the control of EMA in TVC applications to date. Larson[5] has patented an approach to transient force compensation in EMA-TVC actuators. He states in his patent, "A motor responds to transient loads in excess of a predetermined threshold to drive the rocket in a direction of compliance with the transient loads." Larson's statement describes a bilevel approach to transient load compensation. His approach suggests that the actuator should be controlling position until a maximum allowable load is exceeded. When this limit is reached, a force controller is activated to control the actuator force to zero. Hard nonlinearities like those involved in the switching of this bilevel controller are difficult to characterize in terms of both performance and stability. In fact, they are known to cause chatter and other damaging behavior. Doane and Campbell[6] have also produced work involving the use of EMA in TVC applications. They proposed an outer force loop enclosing an inner position control loop. The force error, in effect, produces a position command to the motor. This architecture requires an unreasonably high-bandwidth position controller to adequately compensate for transients that occur at resonance. It would also require either bilevel control similar to that of Larson's approach, or a force controller that is only active during the short periods of startup and shutdown. Unfortunately, neither of the control schemes proposed by Larson and Doane have been validated experimentally. Because the transmitted actuator forces during engine start and stop transients occur at the resonant frequency, a more appropriate control scheme will focus on the frequency of the actuator forces. Such a controller is presented here. It is a linear controller that operates on force frequency rather than force magnitude as the previous researchers suggest.

Doane and Campbell[6] also propose an optimization of the EMA itself. By modifying the roller screw lead and/or the gear ratio, they found that a faster response to any sensed transients can be obtained. Based on simulations of the EMA-TVC system, these authors' optimizations definitely have merit. The work described here, however, focuses on optimizing the controller given an actuator mechanical configuration.

The EMA-TVC system can be characterized by a double-mass-spring-damper model. From a position control standpoint various solutions to the problem of resonance have been suggested for this type of model. A few industrial servo-control card manufacturers propose closing a velocity control loop with the motor (indirect) feedback and implementing the position controller using the direct feedback.[7] In this scheme the velocity loop is a minor loop around which the position controller is implemented. This method gives only marginal improvement and limits the bandwidth of the position controller to frequencies much less than the bandwidth of the velocity loop. A three-lead-network controller, which is essentially implemented as a notch filter using only the direct feedback, has been proposed in the literature.[8] This controller performs very well in the theoretical case where the mechanical dynamics are known very well, are linear, and do not vary with time or position. However, it is not robust with respect to variation of the mechanical dynamics, which is inevitable in any practical situation. Also, these controllers only address the resonance from the closed-loop position-control perspective. They do not address the resonance in response to disturbance inputs.

The work presented in this paper is based on the premise that by reducing resonance in both the position and disturbance responses the EMA-TVC system performance can be improved. The undesirable effects of the engine transients have been attributed to resonance by NASA engineers experienced with the space shuttle, Apollo, and other programs using hydraulic TVC. The transition to supersonic flow in the engine nozzle generates a shock wave[4] that excites any significant resonance in the actuator system. To characterize the start and stop transient forces, instrumented stiff-arms have been substituted in place of the TVC actuators in hot fire tests of engines. The fundamental frequency of the transient forces obtained in the stiff-arm tests has been shown to be a theoretically predicted resonance of the stiff-arm-engine system.[9] Additionally, the transient force data resemble that of an impulse response with the exception that the actual force transients take a few oscillation cycles to build to the highest peak. From this, it is reasonable to suggest that smaller impulse disturbances may exist as a prelude to the larger, more devastating disturbance.

Hardware and Modeling

Figure 2 schematically illustrates the TVC simulator and the experimental hardware used. TVC simulators currently in use by the Component Development Division of the Propulsion Laboratory at NASA Marshall Space Flight Center (MSFC) use an actuator-pendulum configuration. These simulators have been used throughout the U.S. space program in experimentation and control system development for hydraulic TVC actuators. Mounting the actuator in a series with a pendulum captures the greatest majority of the dynamics of an actuator-TVC system by simulating the rocket-actuator movement. All of the experimental data presented here were obtained using a TVC simulator at NASA MSFC with a 1-hp EMA designed for the RL-10 Pratt and Whitney engine.

The major components in the experimental hardware are a Pentium™ PC with an analog/digital interface card for data acquisition and control, a pulse-width-modulated motor controller, the RL-10 1-hp EMA actuator, and the TVC simulator. The motor controller is essentially a transimpedance amplifier, converting an input voltage to a motor current. It contains a high-bandwidth motor-current control loop, which can be treated as a static gain in the lower-frequency mechanical models. Instrumentation includes a resolver mounted on the screw for actuator position, a load cell mounted in the tail of the actuator, motor current sensing in the

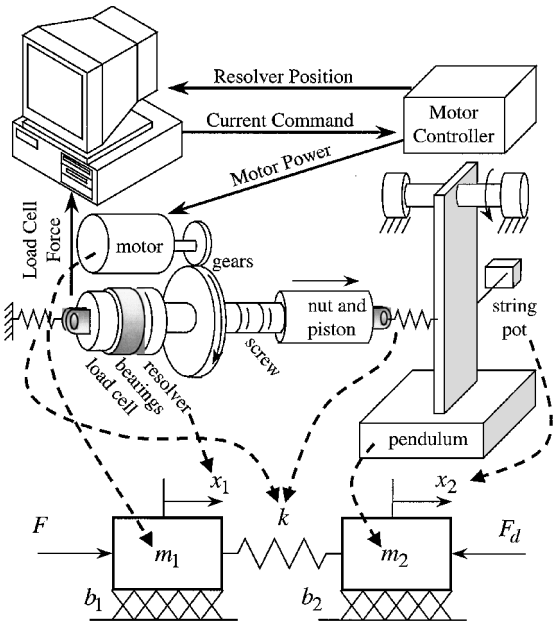

Fig. 2 EMA-TVC simulator and model development.

motor controller, and a string potentiometer attached to the pendulum. In addition, a large impulse hammer with a piezoelectric load cell is used to generate a disturbance impulse force for transient force testing.

Figure 2 also gives a pictorial representation for the model development of the mechanical system. The equivalent translational mechanical system is an intuitive double-mass-spring-damper model. This model captures the dominant dynamic features of the system, as well as important features of more complex aircraft and space structure vibration control problems[8] and many machine tool axes. The modeled spring captures the major cumulative effects associated with the stiffness of actuator attachment points, the pendulum arm (or engine nozzle), torsional windup of the screw, and other actuator components. In past hydraulic-TVC systems the major compliance effects have been attributed to the nozzle, attachment points, and compression of the hydraulic fluid. It has been demonstrated that these effects result in fairly low resonance (as low as 8 Hz) in most hydraulic-TVC systems. Because the stiffness and thus the material composition of the EMA is relatively small, the structural damping in the spring is also small and can be assumed negligible. The following two transfer functions can be used to describe the mechanical dynamics.

$$\frac{x_1(s)}{F(s)} = \frac{m_2 s^2 + b_2 s + k}{s\Delta(s)}$$

where

$$\Delta(s) = As^3 + Bs^2 + Cs + D$$

$$A = m_1 m_2, \qquad B = m_1 b_2 + m_2 b_1$$

$$C = m_1 k + m_2 k + b_1 b_2 \qquad D = k(b_1 + b_2) \tag{1}$$

$$x_2(s)/x_1(s) = k\Big/\left(m_2 s^2 + b_2 s + k\right) \tag{2}$$

The RL10 actuator used in experimentation contains high levels of gear and mount backlash, as well as static friction and amplifier saturation. Detailed simulations are performed using the nonlinear model given by Schinstock et al.[10] and shown in top-level form in Fig. 10. This nonlinear model is used for force reduction analysis in the following sections.

A detailed description of the modeling and estimation of parameters is given by Schinstock et al.[10] For the sake of brevity, the coefficients of the linear model are simply stated without explanation. The linear model coefficients are $k_t = 0.713$ in.-lb/A (0.0804 N-m/A), $N = 0.0062$, $m_1 = 13.8$ lb-s^2/in. (2420 kg), $m_2 = 1.8$ lb-s^2/in. (315 kg), $b_1 = 144$ lb-s/in. (25200 N-s/m), $b_2 = 60$ lb-s/in.(10500 N-s/m), and $k = 48000$ lb/in.(8.4×10^6 N/m).

Controller Development and Design

The linear model introduced in Fig. 3 incorporates only PID position control. To reduce the resonance found in the mechanical system adequately, a DFF compensator is incorporated in the control. This section discusses the design of the PID position controller and, more importantly, the design and theory of the additional DFF compensator used for transient force reduction and resonance reduction. The PID position control is dominant at low frequencies, whereas the DFF dominates the control at frequencies around the resonance. The separation in frequency resolves the issue of competition by the two control loops for plant input (motor current). The final antiresonant controller incorporates both the PID and DFF controllers, which are designed separately. The basis for this will become more evident as the DFF compensator is discussed in more detail.

PID Design

The position controller is designed using a simple rigid body model. This model uses lumped mass and damping without the inclusion of the spring. It is described by the following transfer function:

$$x(s)/F(s) = 1\Big/\left[(m_1 + m_2)s^2 + (b_1 + b_2)s\right] \tag{3}$$

Using the rigid body model, a simplified block diagram is given in Fig. 4.

A specific procedure is given here for the PID design using loop-shaping techniques. The goal of the loop-shaping technique is to obtain an open-loop frequency response with the following characteristics: 1) a high gain at low frequencies to give good tracking at low frequencies, 2) a slope of -20 dB/decade in regions before and after the desired closed-loop bandwidth to give good phase margin and stability, and 3) a zero-dB crossover frequency equal to the desired closed-loop bandwidth.

A PID compensator may be factored into two zeros and a controller gain $[k_d(s + z_1)(s + z_2)/s]$. The two zeros z_1 and z_2 are used to change the slope of the open-loop transfer function (OLTF) at appropriate frequencies, and the controller gain k_d is used to obtain the desired crossover frequency. The design is illustrated in Fig. 5 using the magnitude of the OLTF. One zero is placed according to Eq. (4) to cancel a portion of the plant dynamics. The second zero is chosen in Eq. (5) to be one decade before the desired closed-loop position bandwidth.

$$z_2 = \frac{(b_1 + b_2)}{(m_1 + m_2)} \tag{4}$$

$$z_1 = \omega_{\text{bwp}}/10 \tag{5}$$

Here ω_{bwp} is the target position bandwidth in rad/s.

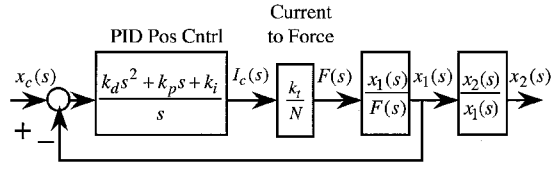

Fig. 3 Comprehensive linear model with PID position control.

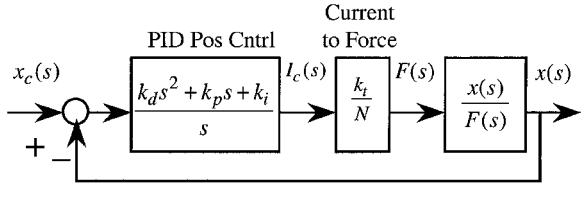

Fig. 4 Simplified position control system with a rigid body model.

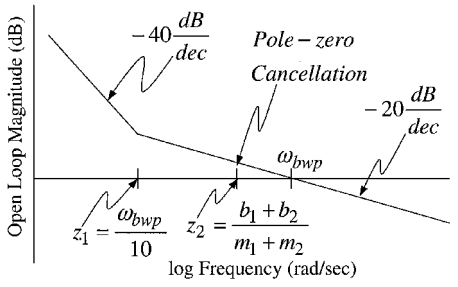

Fig. 5 Loop shape for PID design.

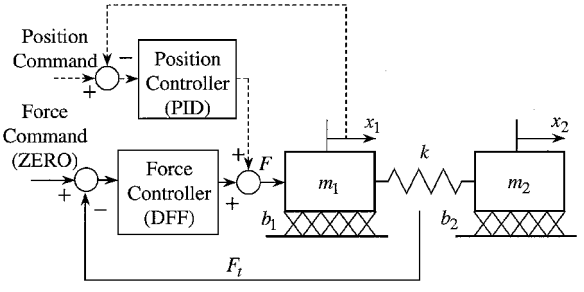

Fig. 6 Conceptual model for DFF controller design.

With the two zeros just given the OLTF from Fig. 4 is

$$G_{\text{olp}}(s) = \frac{k_d k_t (s + z_1)(s + z_2)}{N\left[(m_1 + m_2)s^3 + (b_1 + b_2)s^2\right]} \tag{6}$$

The only unknown in Eq. (6) is the controller gain k_d, which can be found by setting the magnitude of the OLTF at the desired bandwidth frequency equal to one

$$|G_{\text{olp}}(s = j\omega_{\text{bwp}})| = 1 \tag{7}$$

The left-hand side of Eq. (7) is the magnitude of a complex number with an unknown k_d. Solving for k_d will set the crossover frequency for the OLTF to ω_{bwp} and hence approximately set the closed-loop bandwidth to its desired value.

The other PID gains can then be found using the following equations:

$$k_p = k_d(z_1 + z_2) \tag{8}$$

$$k_i = k_d z_1 z_2 \tag{9}$$

The PID controller gains for a 5-Hz bandwidth developed from these procedures are given as follows: $k_p = 68.47$ A/in. (2696 A/m), $k_i = 173.43$ A/in.-s (6828 A/m-s), and $k_d = 4.22$ A-s/in.(166 A-s/m).

DFF Design

The general concept of the DFF compensation is to measure actively the actuator force and to use this measurement in the reduction of the effects of resonance. Physically, a load cell mounted in the tailstock of the actuator is used to measure the transmitted force. The DFF compensator implements a separate force loop in addition to the position control loop already discussed. Figure 6 illustrates the concept of the DFF controller. The PID position controller and the DFF compensator must compete for the plant input. This is an obvious physical conflict because both the transmitted force and the position cannot be controlled independently. This conflict is resolved by designing the DFF compensator to have an effective range only in frequencies near the resonance.

The following relationship between the input force from the motor and the transmitted force in the spring is used as the plant for the DFF design:

$$\frac{F_t(s)}{F(s)} = \frac{k(m_2 s + b_2)}{\Delta(s)} \tag{10}$$

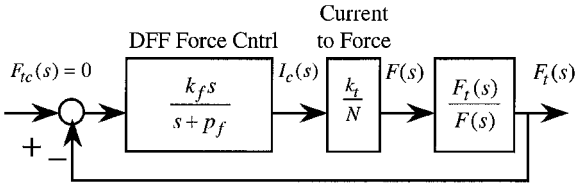

Fig. 7 Block diagram representation of force feedback loop.

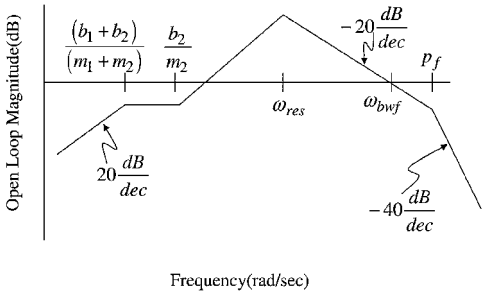

Fig. 8 Loop shape for DFF design

In Eq. (10) $\Delta(s)$ is as defined in Eq. (1). Figure 7 shows the block diagram representation of the force loop with DFF control. It also gives the dynamic structure of the DFF compensator.

The proposed DFF feedback structure was chosen to handle start and stop transients for the following reasons: 1) physical reality—the load cell mounted in the tail-stock of the actuator and the motor position feedback are readily available for control; 2) previous design—the feedback structure is similar to the pressure feedback found in hydraulic systems previously verified and tested by NASA engineers; and 3) high-pass filter structure—the high-pass filter structure of the DFF attenuates the force feedback response at low frequencies while providing a natural peak at the resonance where force should be controlled.

The OLTF of the force feedback loop can be determined from Fig. 7.

$$G_{\text{olf}}(s) = \frac{k_f k_t k(m_2 s + b_2)}{N(s + p_f)\Delta(s)} \tag{11}$$

In Eq. (11) $\Delta(s)$ is as defined in Eq. (1). The goal of the loop-shaping technique used for the design of the DFF compensator is to obtain an open-loop frequency response with the following characteristics: 1) low gain at low frequencies giving poor force control at low frequencies where position control should dominate, 2) peak amplitude at the resonant frequency of the mechanical system, 3) a slope of -20 dB/dec in the region before and after the negative-slope crossover frequency to provide good phase margin and stability, 4) a zero-dB crossover frequency approximately twice the mechanical resonance to provide the force controller with enough gain to control at the resonance, and 5) low gain at high frequencies to reduce the effects of load cell noise and higher-frequency modes generated from other mechanical or electrical resonance.

The structure of the DFF is chosen to include a differentiator and a pole. The differentiator provides low open-loop gain at low frequencies while the pole reduces gain at high frequencies past the resonance. The open-loop magnitude plot is given in Fig. 8. As seen in Fig. 8, the DFF pole p_f is selected beyond the mechanical resonance of the system. It is given as follows:

$$p_f = 10\omega_{\text{res}} \tag{12}$$

where ω_{res} is the mechanical resonance of the system. The force bandwidth frequency ω_{bwf} is chosen somewhat arbitrarily to be twice the resonant frequency.

$$\omega_{\text{bwf}} = 2\omega_{\text{res}} \tag{13}$$

A higher bandwidth will increase the effective range of the force controller but will cause the DFF to compete more with the position controller at low frequencies.

The gain of the DFF controller can be found in a similar manner as that used for the PID gain k_d. With p_f known from Eq. (12), the only unknown in the OLTF for the force loop is the gain k_f. It can be found by setting the magnitude of the OLTF at the desired bandwidth frequency equal to one

$$|G_{\text{olf}}(s = j\omega_{\text{bwf}})| = 1 \tag{14}$$

The DFF compensator parameters developed from the preceding procedures are as follows: $k_f = 0.9758$ A/lb (0.2194 A/N) and $p_f = 1633\ \text{s}^{-1}$.

Combined PID/DFF Loops

Figure 9 illustrates the complete block diagram model of the EMA-TVC system with PID and DFF control combined. It shows that the combination of the two controllers occurs at the current command to the motor controller. The spring force $F_t(s)$ is physically measured with the load cell and fed into the DFF controller. Figure 10 is a diagram from SIMULINK® dynamic systems simulation software, which uses a fourth-order Runga–Kutta integration technique by default. It shows the nonlinear model used to simulate the system. This model includes the nonlinear effects of gear backlash, mount backlash, amplifier voltage saturation, and amplifier current saturation.

Experimental data validating the PID/DFF controller's ability to reduce resonance and transient forces are discussed in the next section. In the remainder of this section, linear models will be used to show that the addition of the DFF compensation to standard PID control removes the resonance in the position control response. And, more importantly, for transient force reduction it will be shown that the DFF also removes the resonance in the transient force response to force occurring on the engine.

Figure 11 illustrates the position control improvement for the engine position x_2. It shows the magnitude of the frequency response of x_2 with respect to the position command x_c. Both plots in Fig. 11 use the gains stated in the preceding design procedure for a desired 5-Hz closed-loop position control bandwidth. Using PID position control alone, the mechanical resonance becomes so significant that it prevents the use of high-bandwidth position controllers. The resonant peak shown for the PID system in Fig. 11

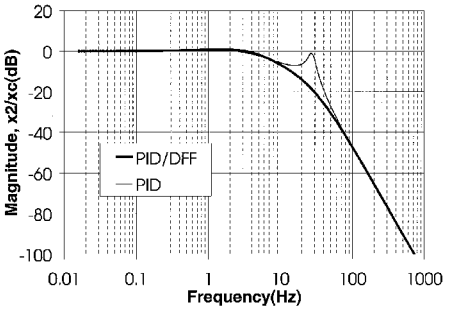

Fig. 11 Magnitude response of x_2/x_c with PID and PID/DFF controllers.

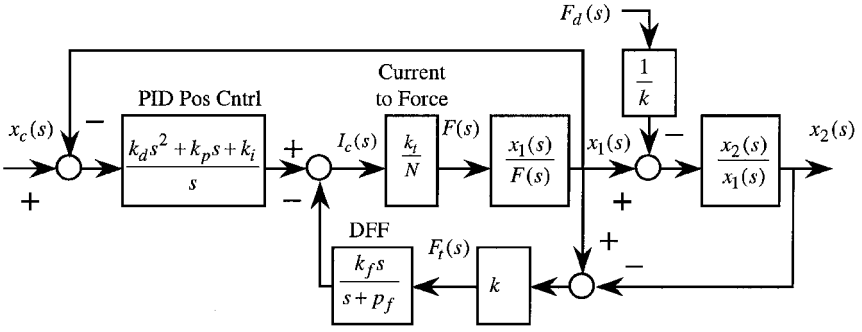

Fig. 9 Comprehensive linear model with DFF and PID control.

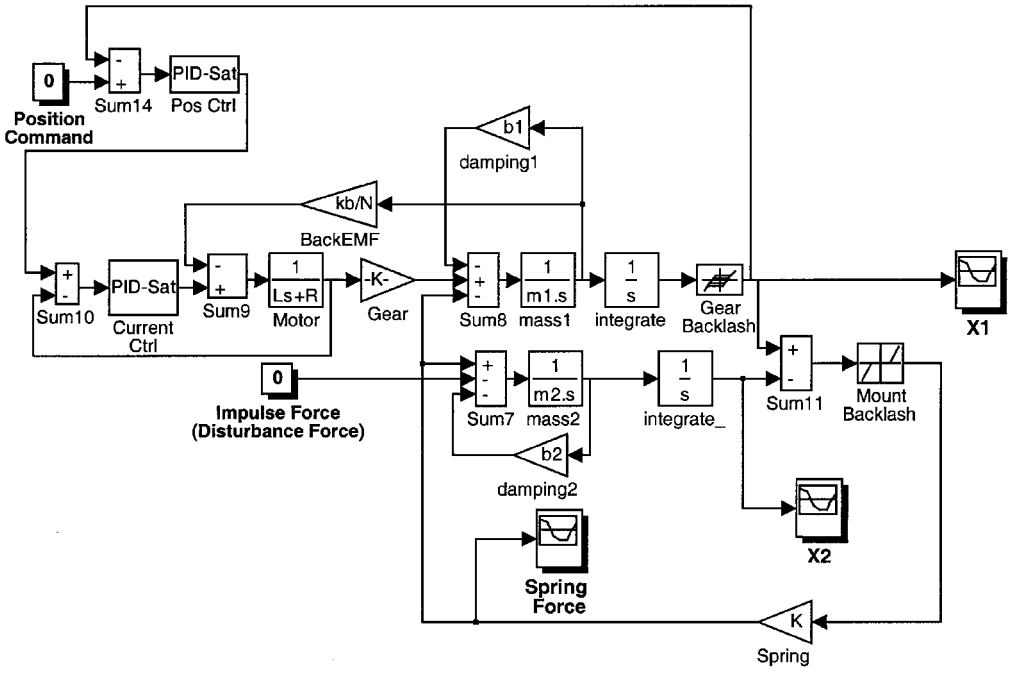

Fig. 10 Comprehensive nonlinear model with DFF and PID control.

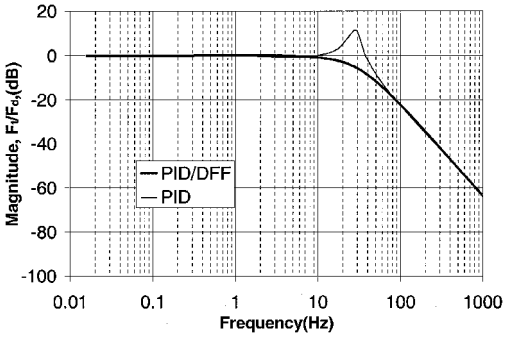

Fig. 12 Magnitude response of F_t/F_d with PID and PID/DFF controllers.

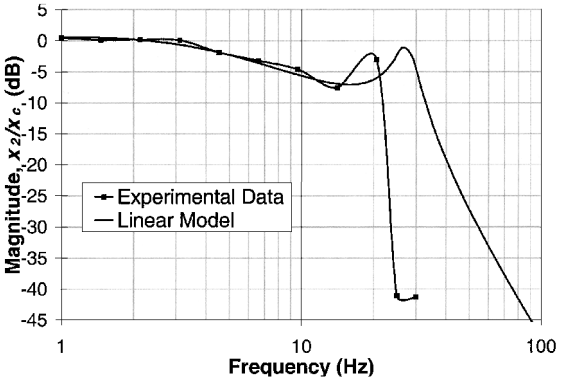

Fig. 13 Experimental and theoretical magnitude response of system with PID control.

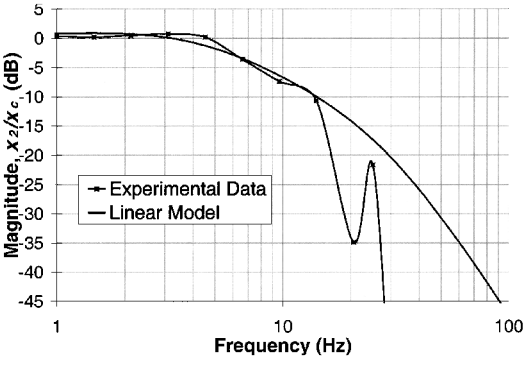

Fig. 14 Experimental and theoretical magnitude response of system with PID and DFF control.

would be unacceptable in most applications. The addition of the DFF controller greatly improves the position control. Using linear models, the DFF completely removes the resonant peak, as shown in the figure.

Figure 12 shows the theoretical magnitude response of the force transmitted in the actuator F_t, with respect to the disturbance force on the engine F_d. In this figure one can see that the PID controller alone results in a resonant peak of 10 dB. This would result in a transmitted force about 3.2 times the input disturbance force at the resonant frequency. On the other hand, the addition of the DFF compensator to PID attenuates the disturbance forces occurring at resonance. At lower frequencies the DFF has no force-reducing properties because the DFF loop was designed to be ineffective at low frequencies so that the PID position controller could be effective.

The combination of reducing the resonance in both the closed-loop position control response and the transmitted force response to disturbances is important. Controllers using a notch filter (or something similar) in the position controller may exhibit the properties shown in Fig. 11 but will exhibit the properties shown in Fig. 12 because such a controller will not actively sense the transmitted force resulting from a disturbance and compensate as the DFF loop does. Furthermore, as will be shown in a following section, the DFF compensation is robust with respect to inaccuracies in modeling of the resonance, whereas a notch filter is not.

Experimental Validation

To validate the performance of the PID/DFF controller, the experimental setup depicted in Fig. 2 is used. First the behavior for the closed-loop position control response in Fig. 11 is shown to be accurate using experimental data for the closed-loop magnitude response for both the PID and PID/DFF controllers. Next, the ability of the DFF loop to reduce transient forces is demonstrated using transmitted force data from impulse hammer strikes on the pendulum. The impulse disturbance force inputs are used because of the practicality of producing sinusoidal input disturbance forces of significant amplitude and frequency. Also, an impulse should be a conservative test for the ability of the DFF to reduce transient forces because the actuator must act immediately to reduce the first peak in the transmitted force rather than reducing the steady-state oscillation produced by a sinusoidal input.

Experimental data are presented in Figs. 13 and 14 along with the linear models for predicting the closed-loop position control response. Each data point is shown with a discrete point, and smoothed curves are added to allow reasonable interpretation. Each data point was generated using the following procedure. A sinusoidal input with the desired frequency was generated digitally in the control computer for the position command x_c. While feeding this command into the control system, the command and the response x_2, were recorded simultaneously in the control computer, using the analog voltage signal from the string potentiometer for measurement of the response. The first 10 cycles of each sinusoid were eliminated from the data to alloy the response to reach steady state. The command and response data were then reduced using a fast Fourier transform to obtain the magnitude and phase of each of the signals at the driving frequency. The magnitude ratios are shown in the figures. Although the phase correlates well with what would be expected from the magnitude plots, they are not shown for the sake of brevity. The location of the resonant peaks indicated in the data correlated with obvious audible and visual indications of the resonance.

Results shown in Figs. 13 and 14 validate the linear model for predicting the closed-loop position control response. The linear model data presented in these two figures are the same as that presented in Fig. 11. It is compared to experimentally acquired data with good correlation except at high frequencies. The amplitude of the sinusoidal inputs was 0.1 in. at all frequencies except near the resonance in the system with PID control only, where a smaller amplitude was used to prevent damage to the hardware. With the DFF the amplitude was kept constant because of the DFF's ability to reduce the effects of resonance. Even during these early stages of testing, it was obvious that the DFF compensator protects the hardware from damage. Comparing resonant peaks for the experimental data in two figures shows that it is reduced by a factor of about 20 dB. This is a factor of 10 in magnitude ratios.

Figure 13 indicates there is a difference between the resonant frequencies of the model and actual system. Comparing the resonant frequencies in the two figures suggests that the resonance is shifted to a higher frequency by the addition of the DFF. Also, the high-frequency data, where severe attenuation occurs, are significantly different from the linear model in both Figs. 13 and 14. All of this might be explained by backlash in the actual system demonstrated in Fig. 15, which cannot be included in the linear model. These data suggest that the nonlinear model might be required to capture some additional dynamics. However, nonlinear models are quite time consuming and difficult to develop. Although the actual system has significant nonlinearities, the linear models were sufficient for control system design using the methods presented here.

An impulse hammer was used to develop impulse data that verify the DFF's ability to reduce the forces transmitted in the actuator. An impulsive strike at the back of the pendulum produces transmitted

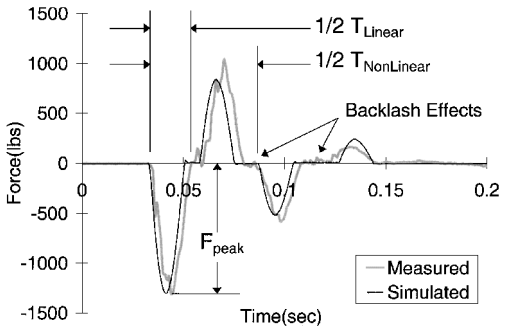

Fig. 15 Measured and simulated transmitted force caused by a hammer impulse.

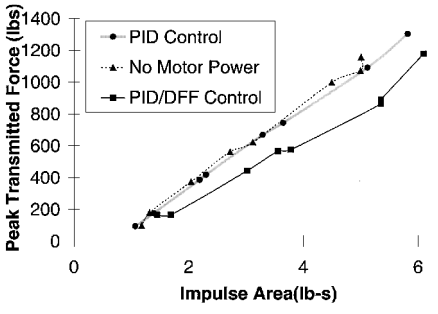

Fig. 16 Peak transmitted force caused by a hammer impulse.

force data like those shown in Fig. 15, a nonlinear impulse response. Figure 15 shows the results of a simulated impulse response using the nonlinear model (Fig. 10) of the TVC-EMA system along with an experimentally measured response with the same impulse area. This figure shows that the nonlinear model provides a very accurate representation of the nonlinear effects within the system. As the amplitude of the oscillation decreases, the frequency also decreases. This may explain the shift in resonance between the linear model and the experimental data in Fig. 13. The figure also demonstrates that at low amplitudes where the backlash is a very important part of the response a linear model would not be very accurate. This agrees with the high-frequency data in Figs. 13 and 14.

Typically, the estimation of inertia and motor parameters in EMAs is somewhat trivial because of the availability of manufacturing documentation. The spring rate k is perhaps the most difficult to estimate with the actuator attached to an engine. This is, in part, because of the dominant resonance is caused by the compliance in the engine-actuator mounting and engine nozzle, which is typically very difficult to measure and/or calculate. Additionally, nonlinear backlash effects cause the resonance to shift.

Figure 16 illustrates the transient force reduction properties of the DFF controller with data resulting from various size-single impulse disturbances. Each data point in Fig. 16 is the peak force measured for the impulse disturbance. The transient force data for each impulse test resemble that in Fig. 15. Figure 15 shows, using data from realistic EMA-TVC hardware, that the maximum transmitted force resulting from an impulse is reduced by approximately 20% with the addition of the DFF compensator. It has been verified using simulations with the nonlinear model that motor-current saturation has limited the amount of reduction obtained with the DFF for impulse input forces.

Figure 16 suggests a ratio of 0.8 for the transmitted force in the PID/DFF system to the transmitted force in the PID system. However, Fig. 12 suggests a ratio of approximately 0.17 (−15 dB) at resonance. These two ratios are significantly different measures of the ability of the DFF to reduce the transmitted force. The first is found using the first peak of an impulse response, and the second is found from the amplitude of a steady-state oscillation. The true ratio will depend on the character of the input disturbance force. For the engine start and stop transients the true ratio might be expected to lie somewhere in between the values just given. The engine transients have been modeled both as single-impulse inputs and as a series of a few impulses separated by the period of the resonant frequency. The latter seems to reproduce more accurately the transmitted forces observed in stiff-arm tests described in the Introduction.

Robustness of the DFF

As already discussed, the controller design uses an estimate of the spring constant to capture the resonance directly in design. And, as shown in the preceding section and in Ref. 10, the spring rate and resonant frequency can be difficult quantities to estimate accurately. Varying the spring constant while maintaining the controller gains found in the design using a 26-Hz resonance estimate performs a simple but effective analysis of the sensitivity of the system. This demonstrates the effectiveness of the DFF controller with large deviations in the spring constant. Equation (15) gives an approximate spring constant for a given resonant frequency provided that m_1 is considerably larger than m_2

$$k \cong m_2 \omega_{\text{res}}^2 \tag{15}$$

This relation is used in this section to estimate a spring rate for a given resonance.

The frequency response of the transmitted force with respect to the disturbance force can be generated using the linear model with various values for k. Figure 17 shows the magnitude of the transmitted force with the PID controller. Figure 18 is a similar plot using the PID and DFF control loops. In both of these figures, all other coefficients are as already stated.

The results in Fig. 17 are as might be expected. As the modeled resonance varies, so does the resonant peak in the response. Figure 18 demonstrates that DFF compensator is robust with respect to variation of the spring rate and resonance. This is an intuitive result considering that the physical plant, rather than the controller, determines the location of the peak amplitude of the open-loop gain in Fig. 8. If the additional feedback from the load cell were not used, it would be difficult to obtain a system as robust as this. Similar results are obtained for the same type of analysis of the closed-loop position control response.

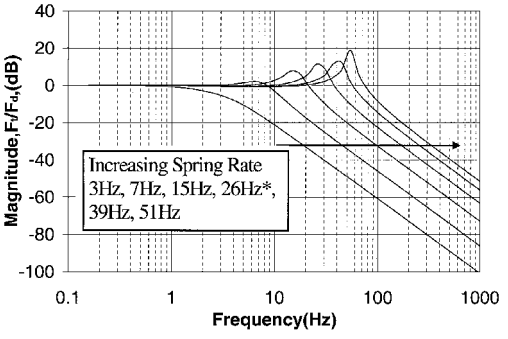

Fig. 17 F_t/F_d magnitude response with varying k and PID control.

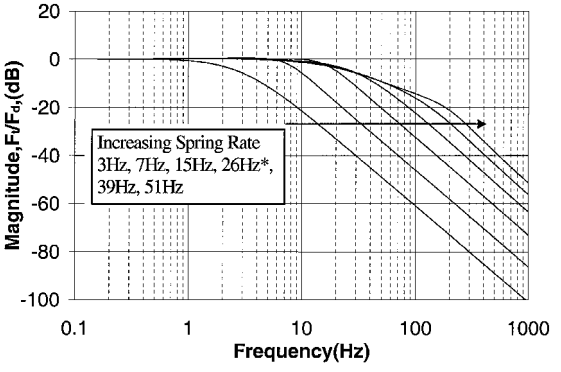

Fig. 18 F_t/F_d magnitude response with varying k and PID/DFF control.

Conclusions

Addition of the DFF compensator to PID position control has been shown as an excellent solution to the resonance problem in EMA-TVC systems. The experimental results from a realistic hardware simulator of an EMA-TVC system illustrate that the DFF lowers the transient forces while allowing a high-bandwidth position controller without significant resonance. The theoretical results match the experimental findings and indicate that the proposed control techniques are robust.

For an EMA-TVC system similar to the TVC simulator, the theoretical and experimental results indicate that a reduction between 80 and 20% might be expected in the actuator forces experienced during engine start and stop transients. The amount of reduction would be dependent on the character of the transients experienced. If the transmitted forces take a few oscillation cycles to build to a peak, then a greater reduction than the 20% approximation obtained from the impulse tests might be expected. This is a reasonable expectation given the transmitted force data from previous stiff-arm tests, which does take a few cycles to build to a peak.

In the closed-loop position control response a 20-dB reduction in the resonant peak was obtained experimentally with the addition of the DFF to standard PID control with the same bandwidth. This is an important result even without the added benefit of transmitted force reduction. It allows the control system designers the luxury of obtaining a higher-performance EMA-TVC system without the cost of lightly damped, potentially dangerous system characteristics.

Continuing efforts in EMA development will probably focus mainly on power generation/storage, although some work will undoubtedly focus on controls and actuator design. The large electric power requirements of the increased usage of EMA and the power transients they cause are major concerns. Detailed understanding of the mechanisms of regeneration in motor controllers and the capture of regenerative energy are also important. A few actuators already include redundancy in the form of multiple motors, and control of such actuators will have to be studied in detail.

Acknowledgments

The work described here was supported in part by a NASA/ASEE Faculty Fellowship and a NASA/ASEE Accompanying Student Fellowship. It has also been supported by NASA Grant NAG8-1407 to the University of Alabama Electromechanical Actuation Test Facility.

References

[1]Trosen, D. W., and Cannon, B. J., "Electric Actuation and Control System," *Proceedings of the 31st Intersociety Energy Conversion Engineering Conference*, Vol. 1, Inst. of Electrical and Electronics Engineers, New York, 1996, pp. 197–202.

[2]Burrows, L. M., and Roth, M. E., "Electromechanical Actuation System for an Expendable Launch Vehicle," *Proceedings of the 27th Intersociety Energy Conversion Engineering Conference*, Vol. 1, Inst. of Electrical and Electronics Engineers, New York, 1992, pp. 251–255.

[3]Kaiser, D. A., Morris, J., and Durkin, C., "Dynamic Models Show the Effects of Different Couplers on Motion System Response in Drivescrew Applications," PCIM, *Power Conversion and Intelligent Motion*, Vol. 23, No. 6, Intertec International Inc., Ventura, CA, 1997, pp. 84–90.

[4]Ryan, R. S., "Problems Experienced and Envisioned for Dynamical Physical Systems," NASA-TP-2508, Aug. 1985.

[5]Larson, R. K., "Actuation with Active Compensation for Transient Loads," United States Patent, Patent 5560559, Oct. 1996.

[6]Doane, G., and Campbell, W., "Advanced Electric Motor Flux Mapping," NAS 1.26:184317, NASA-CR-184317, April 1992.

[7]Tal, J., "Ask Jacob Tal," *Servo Trends: A Quarterly Newsletter Published by Galil Motion Control Inc.*, Vol. 14, No. 3, 1998, p. 4.

[8]Chiang, R. Y., and Safonov, M. G., "H^{∞} Robust Control Synthesis for an Undamped, Non-Colocated Spring-Mass System," *Proceedings of the American Control Conference*, American Automatic Control Council, Evanston, IL, May 1990, pp. 966, 967.

[9]Haskew, T. A., and Schinstock, D. E., "Final Report: Design and Application of Electromechanical Actuators for Deep Space Missions," Final TR for NASA Grant NAG8-240, Univ. of Alabama, BER Rept. 632-163, Tuscaloosa, AL, May 1996.

[10]Schinstock, D. E., Scott, D. A., and Haskew, T. A., "Modeling and Estimation for Electromechanical Thrust Vector Control of Rocket Engines," *Journal of Propulsion and Power*, Vol. 14, No. 4, 1998, pp. 440–446.